Evaluation of Vehicle Camouflage Effectiveness Under a Complex Background Based on the Time-Limited Search Model

Dong Wang ⓘ, Qinhe Gao ⓘ, Zhihao Liu, Yao Ding ⓘ, Tong Huang, and Lei Gao

Abstract—To comprehensively evaluate the camouflage effect of a camouflaged vehicle in a complex background based on the detection and identification processes of the time-limited search model, the visual saliency degree and feature similarity degree were used to represent the camouflage effect, and a camouflage effect evaluation method was proposed. For the visual saliency degree algorithm, in which the concepts of local saliency degree and target saliency degree were introduced, the visual saliency features of the camouflaged vehicle and background image were manually extracted, multiscale saliency matrices were constructed, and the comprehensive saliency function was used to calculate the visual saliency degree. Based on the bag of visual words model, the feature similarity degree algorithm extracted the local features from public images of the camouflaged vehicles, clustered these features to form a visual word bag, and calculated the feature similarity degree by comparing the local features of the camouflaged vehicle with the visual word bag. Through experimental verification and analysis of the results, the method considering complex landform background characteristics, battlefield target reconnaissance processes, and different camouflage statuses of the vehicle could objectively obtain the camouflage effect value of vehicles, quantitatively determine the advantageous application environment of different camouflaged states, and provide data support for camouflaged state design and concealed area selection.

Index Terms—Camouflage effectiveness, evaluation, saliency degree, similarity degree, time-limited search model.

I. INTRODUCTION

IN MODERN warfare, high-frequency detection on the battlefield has been revisited using various sensors (e.g., visible light, infrared, hyperspectral, and radar) mounted on a variety of observation platforms (e.g., satellites, reconnaissance planes, and drones) [1], forming two-dimensional (2-D) digital graphics with multispace, multitime, multiesolution [2], and multipolarization [3] in real time to detect and identify the regions of interest (ROIs) and targets of interest (TOIs) [4]. Therefore, to

achieve a better camouflage effect in complex regions, a vehicle should not be located in the ROI and should not become a TOI to reduce the probability of detection as much as possible. Additionally, the public features of the vehicle should be covered and hidden as much as possible to reduce the probability of being identified [5]. Based on this, the evaluation of the vehicle's camouflage effect should consider the possibility of becoming a TOI and the exposure degree of the public features.

According to the classification of the evaluation levels of the weapons system in the U.S. MIL-STD-721B document [6], the evaluation levels of camouflage of vehicles can be divided into measures of camouflage performance (MOCP), measures of camouflage ability (MOCA), and measures of camouflage effectiveness (MOCE). Here, MOCP is a quantitative parameter reflecting antireconnaissance properties, such as reflectivity and reflection cross section, which is determined by the inherent physical structure parameters of the vehicle. MOCA, which refers to the antireconnaissance ability of vehicle MOCP in a certain detection environment, is the set of capability levels formed by inherent performance in different detection environments and reflects the manifestation of camouflage performance in a specific detection environment. MOCE refers to the possibility of successful concealment of vehicles in the battlefield dynamic detection environment, which is comprehensively affected by its camouflage performance, battlefield detection environment, and mission requirements. In this article, the camouflage effectiveness of vehicles is evaluated based on this definition.

Camouflage effectiveness evaluation research on weapons has mostly concentrated on camouflage patterns [7]–[9], infrared detection [10]–[12], hyperspectral image processing [13]–[15], coating materials [16]–[18], and is used in different aspects to evaluate camouflage performance or individual ability. However, few studies have evaluated camouflage effectiveness in combination with combat tasks, complex terrain, and reconnaissance means.

In this article, with reference to the time-limited search (TLS) model [4], a camouflage effect evaluation model is constructed by integrating the saliency of the vehicle becoming TOI in the battlefield background image and the similarity of the camouflaged vehicle to public features, and the camouflage effectiveness of the vehicle is analyzed. In calculating the camouflaged vehicle saliency degree (SAD) in the background image, the target saliency model of the human visual attention mechanism is
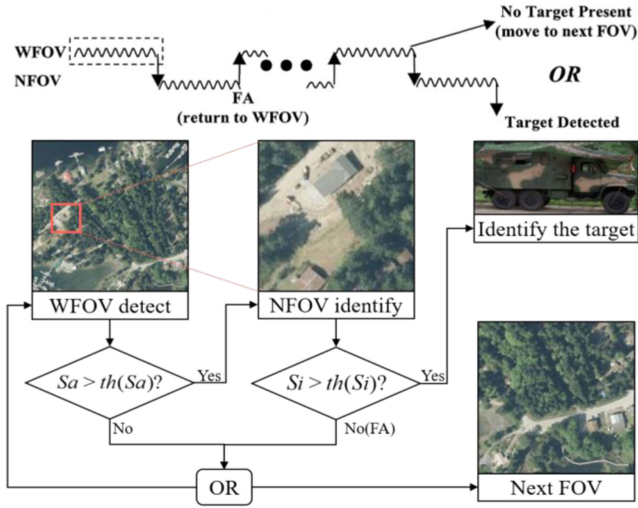
Fig. 1.   Camouflaged target search process.

adopted to extract features manually for comparison calculation. The similarity degree (SID) between camouflaged vehicle images and public features adopts the bag of visual words (BOVW) model, which can describe local vehicle features and has high efficiency in content-based similarity calculations.

The main contributions of this article are as follows.

1) A camouflage effectiveness evaluation method is proposed based on the TLS model for a camouflaged vehicle in a complex landform background.

2) The camouflage effectiveness is evaluated by combining the SAD and SID of the camouflaged vehicle.

3) It is proven that the method can analyze the advantages and disadvantages of different camouflaged states and landform backgrounds, and provide quantitative support for decision-making.

II. OVERVIEW

An overview of our proposed camouflage effectiveness evaluation method is shown in Fig. 1. This method is based on the TLS model. In TLS, each camouflage vehicle search process consists of two steps. First, the detection system searches for ROIs and TOIs in a wide field of view (WFOV), which is called the target detection process (TDP). Then, the detection system searches in the narrow field of view (NFOV), where the ROIs or TOIs are located for recognition and confirmation. The detected target is compared with the target public features to confirm the type and details of the target, which is called the target identification process (TIP). Only after the target is identified can its operational value and attack assessment be determined, and the whole search process is completed.

From the perspective of the human visual attention mechanism [19], the key factor affecting the TDP is the saliency of ROIs or TOIs in the WFOV, which includes the saliency of different background regions and the saliency of a target relative to the background, which is called the local saliency degree (LSAD) and target saliency degree (TSAD), respectively. The key factor affecting TIP in NFOV is the similarity between the
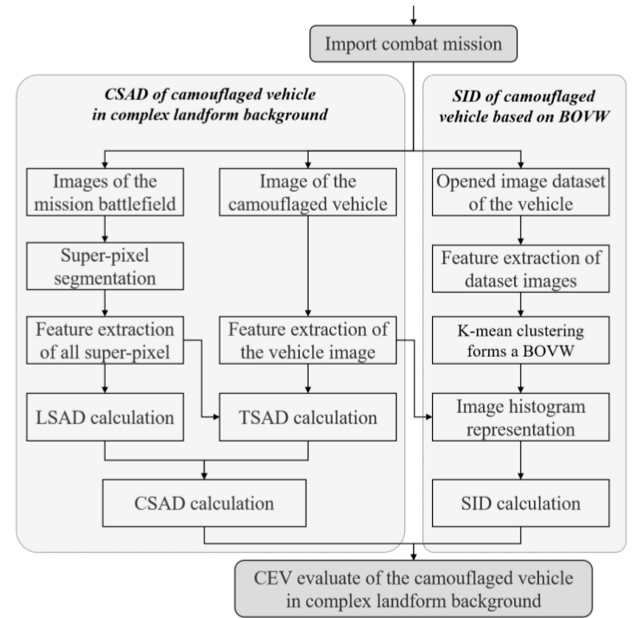

Fig. 2.   Camouflage effectiveness evaluation method.

detected target and the public features of the target. Accordingly, we propose a camouflage effectiveness evaluation model for vehicles in a complex background under TLS, as shown in Fig. 2.

The method starts with the combat mission. Then, the background image, the camouflaged vehicle image, and the vehicle public image dataset are input, and the method proceeds as follows.

1) Superpixel segmentation is performed on the background image, features with all superpixels are extracted, the feature distance between each superpixel is calculated, and the adjacent superpixel comparison model is used to form the LSAD of each region of the background image after normalization.

2) The features of the camouflaged vehicle image are extracted, the feature distance between each superpixel and the vehicle image is calculated, and the TSAD after normalization is formed.

3) The comprehensive saliency degree (CSAD) function is used to calculate the CSAD of the camouflaged vehicle in each superpixel/area of the background.

4) The local features of all images in the dataset of the public vehicle images are extracted and clustered to form a visual dictionary.

5) The local features of the camouflaged vehicle image are extracted and compared with the visual words in the visual dictionary to obtain the SID.

6) The CSAD and SID are integrated to evaluate the vehicle camouflage effectiveness value (CEV) by using the following equation:

$$E = 1 - Sa \cdot Si \tag{1}$$

where E is the CEV of the vehicle, and $E \in [0 1]$. The larger the value is, the better the camouflage effectiveness. Sa is the CSAD
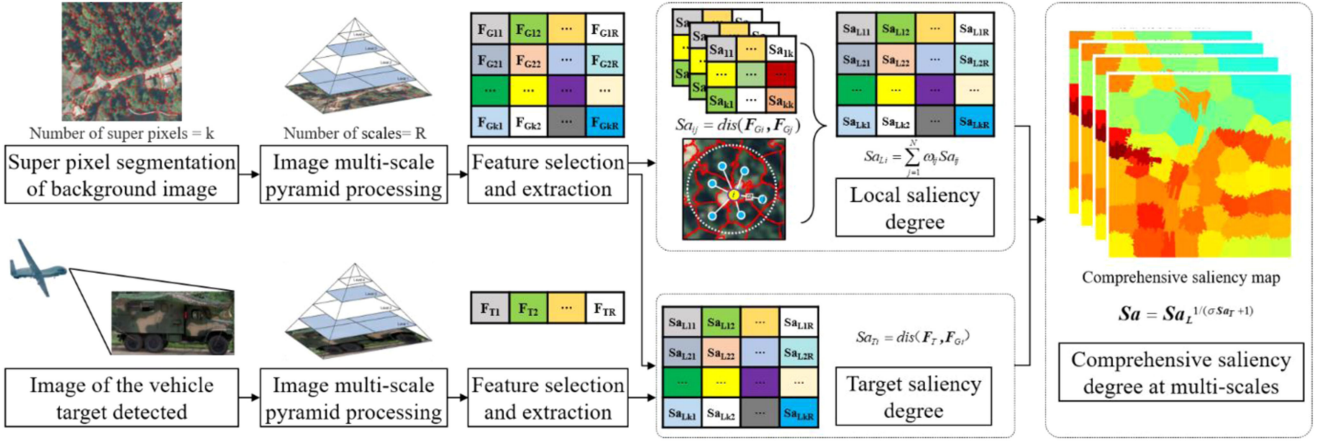
Fig. 3. Vehicle comprehensive saliency degree algorithm.

of the camouflaged vehicle, and Si is the SID of the camouflaged vehicle.

III. CSAD ALGORITHM

Whether a camouflaged vehicle is easy to detect and becomes a TOI in a complex background depends on its CSAD, which consists of two parts. One part is the LSAD, which represents the visual feature saliency of the vehicle's area relative to the whole background image. The second part is the TSAD, which is the visual feature saliency of the camouflaged vehicle relative to the local area of the background. Therefore, the CSAD algorithm of the camouflaged vehicle in the complex background is proposed, as shown in Fig. 3, and proceeds as follows.

1) The visual saliency features are manually selected and the feature distance representation method is determined.
2) Superpixel segmentation is performed on the background image.
3) The multiscale features of each superpixel of the background image and the camouflaged vehicle image are extracted.
4) The feature distances between superpixels at different scales are calculated, and the LSAD is calculated by using the adjacent superpixel comparison model.
5) The feature distance between the camouflaged vehicle image and each superpixel is calculated at different scales and normalized to form the TSAD.
6) The CSAD function is used to calculate the CSAD of the camouflaged vehicle in each superpixel/region of the background.

A. Superpixel Segmentation of the Background Image

Superpixel segmentation divides adjacent pixels with similar features into image blocks with a certain homogeneity. Superpixel blocks are taken as the basic unit to express image features instead of a large number of pixels, which can greatly reduce the complexity of image processing. In the evaluation of camouflage effectiveness, the area where the camouflaged vehicle is located mostly contains uneven landforms such as forestland, roads, and scattered dwellings. A proper number of
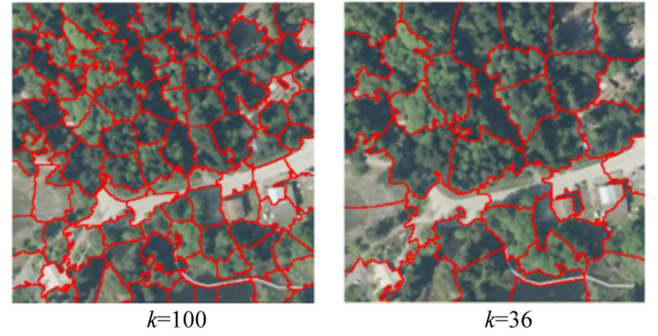

Fig. 4. Image segmentation with different numbers of superpixels.

superpixel blocks is used to express the complex ground object background, which reduces the complexity of image processing, ensures the evaluation dimension, and enables feature mining of limited background images.

Commonly used superpixel segmentation algorithms mainly fall into two categories: those based on the graph theory method and those based on the gradient descent method. In this article, the simple linear iterative clustering (SLIC) algorithm based on the gradient descent method is used for saliency detection [20].

For SLIC segmentation of the background image, the size of the superpixel is determined according to the length l of the vehicle. The step size is $S = 2l$, the number of superpixels is $K = \text{floor}(N/4l^2)$, and N is the total number of image pixels. Fig. 4 shows an example of the segmentation results of the background with different superpixel numbers.

B. Saliency Feature Selection and Distance Representation

Human visual saliency models can be divided into two types: bottom-up (UP) and top-down. The detection and identification of camouflage vehicles under complex backgrounds requires high real-time performance and rapidity, and the UP model based on data-driven, task-free, and prior knowledge has stronger adaptability. The current classical visual saliency model and its algorithm are shown in Table I.

In view of the existing visual SAD algorithm, the exposure features of camouflage vehicles, and the difference between

TABLE I
CLASSIC VISUAL SALIENCY MODELS AND THEIR ALGORITHMS

Model	Algorithm Description
Itti[21]	Perform a "peri-center difference" operation on the brightness, color, and texture of the RGB image.
GBVS[22]	Steady-state balance is used as a measure of the salience of the brightness, color, and texture of the image.
SR[23]	The 2D discrete Fourier transform is applied to the image, and the spectral residuals of the log-amplitude spectrum are calculated in the frequency domain.
AC[24]	The Euclidean distance between the three channel eigenvalues and the mean values of all pixels of the CIE-Lab image.
FT[25]	Through frequency domain filtering, the low-frequency part reflecting the overall information of images is obtained, and the Euclidean distance between images is calculated in the CIE-Lab space.
CA[26]	The Euclidean distance of the three channel values and the spatial distance between pixels of the CIE-Lab image are weighted and integrated to obtain the SAD.
MSS[27]	The Euclidean distance between the mean values of three channels and their fixed neighborhood in the CIE-Lab image are obtained.
SF[28]	The color uniqueness is weighted by spatial distance, and the spatial color distribution is weighted by color similarity. Then, the SAD of the segmented image is obtained by combining the two sides.

TABLE II
SALIENCY FEATURES AND THEIR DISTANCE

Saliency features	Feature distance
Brightness of CIE-Lab space, value of the L channel[29]	$D_1 = |L_x - L_y|$
Color in HSV space[30], quantization histogram of the three HSV channels	$D_2 = 1 - \sum_{i=1}^{300} min(H_x(i), H_y(i))$
Hu moment of gray image[31], the feature vector formed by the 7 Hu moments	$D_3 = \|F_{Hux} - F_{Huy}\|$
Color moments of RGB image[32], the feature vector formed by the third-order color moments	$D_4 = \|F_{colx} - F_{coly}\|$
GLCM texture of gray image[33], The feature vector formed by the 6 quadratic statistics	$D_5 = \frac{\sum_{i=1}^{4}\|F_{tx}^{(i)} - F_{ty}^{(i)}\|}{4}$
SSIM structure of gray image[34], The structural similarity index measure	$D_6 = 1 - \frac{(2\mu_x\mu_y + C_1)(\sigma_{xy} + C_2)}{(\mu_x^2 + \mu_y^2 + C_1)(\sigma_x^2 + \sigma_y^2 + C_2)}$
LBP based on DCT[35], Local binary pattern feature in the low frequency spatial domain	$D_7 = \|F_{LBP1}^{(DCT)} - F_{LBP2}^{(DCT)}\|$
LBP based on SR[23], LBP feature of image spectral residuals in the space domain	$D_8 = \|F_{LBP}^{(SR)} - F_{LBP}^{(SR)}\|$
The pHash based on SR[23], The pHash feature of image spectral residuals in the space domain	$D_9 = \|F_{pHash}^{(SR)} - F_{pHash}^{(SR)}\|$

complex background and vehicle image features, in this article, nine-dimensional (9-D) features of the background and the camouflaged vehicle images are extracted from statistical features, structural features, and frequency-domain (FD) features to calculate the CSAD, as shown in Table II.

C. Adjacent Superpixel Comparison Calculation Model

In a background image, the LSAD of a certain superpixel depends on the feature difference between it and the surrounding superpixels. Therefore, the adjacency superpixel comparison model [36] can be used to calculate the LSAD of the local area of the background, as shown in Fig. 5.
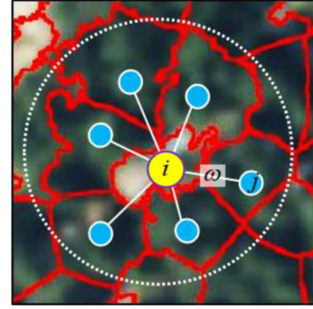

Fig. 5.   Adjacent superpixel comparison model.

In the figure, the yellow point is the central superpixel, and the superpixels that share an edge with it, i.e., the adjacent superpixels, are represented by the blue points. A one-layer adjacent superpixel comparison calculation model is formed with the central node, N adjacent nodes, and N connected edges, where N is the number of adjacent superpixels. The blue node j represents the significant feature distance between adjacent superpixel j and central superpixel i. The connected edge of nodes represents the influence weight ω of the adjacent superpixel on the SAD of the central superpixel, which is constrained by the size of the blue node; i.e., the larger the feature distance is, the larger the weight.

The LSAD of central superpixel i relative to N adjacent superpixels is expressed as follows:

$$S a_{Li} = \sum_{j=1}^{N} \omega_{ij} D_{ij} \qquad (2)$$

where $D_{ij} = dis(F_{Gi}, F_{Gj})$ is the normalized value of the distance between the feature vectors F_{Gi} and F_{Gj} of superpixels i and j, respectively, and weight $\omega_{ij} = D_{ij} / \sum_j D_{ij}$, $\sum_j \omega_{ij} = 1$.

D. CSAD Function

The TSAD is represented by the feature distance between the camouflaged vehicle image and the background superpixel where the vehicle is located. The camouflaged vehicle image and background image are homogenized to make the camouflaged vehicle image format, resolution, and size match the background image. The distance between the feature vector F_T of the camouflaged vehicle image and the background superpixel feature vector F_{Gi} are is calculated, and the TSAD is obtained after normalization

$$Sa_T = dis(F_T, F_{Gi}). \qquad (3)$$

The LSAD of Sa_L and the TSAD of Sa_T form a 2-D vector space $V = \text{Span}\{Sa_L, Sa_T\}$, where $Sa_L \in [0, 1]$, $Sa_T \in [0, 1]$.

The CSAD is a set of functions from the 2-D vector space V to the real number field Sa, and $Sa \in [0, 1]$. Therefore, the CSAD function can be expressed as

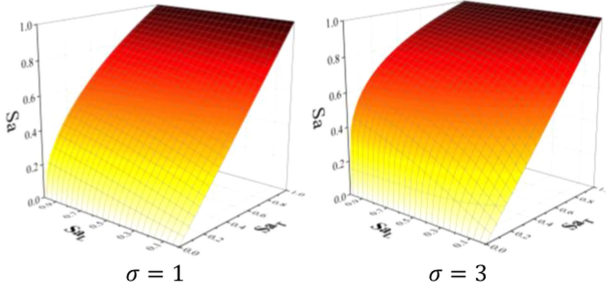$$J[Sa] = \int_0^1 \int_0^1 F(Sa_T, Sa_L) \, dSa_T dSa_L. \qquad (4)$$

Fig. 6. CSAD function.

When both Sa_L and Sa_T are 1, Sa is 1. When Sa_T is 0, Sa is 0. When Sa_L is 0, Sa equals Sa_T. When Sa_T is 1, Sa is 1. Therefore, the CSAD function satisfies the boundary constraint condition

$$\text{st.} \begin{cases} 0 \leq f(Sa_T, Sa_L) \leq 1 \\ f(11) = 1 \\ f(0, Sa_L) = 0 \\ f(Sa_T, 0) = Sa_T \\ f(1, Sa_L) = 1 \end{cases}. \tag{5}$$

In addition, through saliency influence relationship analysis, the larger Sa_L is, the more obvious the cumulative effect on Sa_T. In the Sa_T and Sa_L directions, Sa increases monotonically; i.e., the gradients in both directions are not less than 0. Based on the analysis of boundary conditions and influence relations, the power function is selected for computer iterative checking, and the CSAD function can be expressed as

$$Sa = \mathrm{Sa}_T^{1/(\sigma \mathrm{Sa}_L + 1)}, \sigma \geq 1. \tag{6}$$

Here, σ is the influence intensity factor of the LSAD, which is related to the background complexity. The more complex the landform is, the more obvious its influence on CSAD, as shown in Fig. 6.

E. Matrix Form of the CSAD

Multiscale comparison of background and camouflaged vehicle images with different resolutions can better reflect the salience of the camouflaged vehicle. At each scale of the image with R scales, the background image is divided into k superpixels, and the camouflaged vehicle image of the corresponding scale is compared with k superpixels to form R feature distance matrices. At the scale of r ($r \in \{12, \ldots, R\}$), the feature distances between k superpixels of the background constitute a symmetric matrix of $k \times k$

$$D_{\mathrm{Ln}}^{(r)} = \begin{bmatrix} 0 & D_{21}^{(r)} & \cdots & D_{k1}^{(r)} \\ D_{12}^{(r)} & 0 & \cdots & D_{k2}^{(r)} \\ \vdots & \vdots & \ddots & \vdots \\ D_{1k}^{(r)} & D_{2k}^{(r)} & \cdots & 0 \end{bmatrix}. \tag{7}$$

Using the adjacency superpixel comparison model, the LSAD matrix of background images at R scales is obtained

$$S a_L = \begin{bmatrix} Sa_{L11} & \cdots & Sa_{LR1} \\ \vdots & \ddots & \vdots \\ Sa_{L1k} & \cdots & Sa_{LRk} \end{bmatrix}. \tag{8}$$

The feature distances of each scale between the vehicle image and k superpixels of the background constitute the camouflaged vehicle distance matrix

$$D_T = \begin{bmatrix} D_{T11} & \cdots & D_{TR1} \\ \vdots & \ddots & \vdots \\ D_{T1k} & \cdots & D_{TRk} \end{bmatrix} \tag{9}$$

which is the TSAD matrix

$$S a_T = D_T = \begin{bmatrix} Sa_{T11} & \cdots & Sa_{TR1} \\ \vdots & \ddots & \vdots \\ Sa_{T1k} & \cdots & Sa_{TRk} \end{bmatrix}. \tag{10}$$

The R dimension vectors of the TSAD matrix and the LSAD matrix can be expressed as

$$S a_T = \begin{bmatrix} Sa_T^{(1)} & \cdots & Sa_T^{(R)} \end{bmatrix} \tag{11}$$

$$S a_L = \begin{bmatrix} Sa_L^{(1)} & \cdots & Sa_L^{(R)} \end{bmatrix}. \tag{12}$$

The matrix form of the CSAD obtained by the CSAD function is

$$Sa = Sa_L^{\frac{1}{\sigma Sa_T + 1}}, \sigma \geq 1. \tag{13}$$

IV. SID ALGORITHM

Only after identifying the type of TOI in the NFOV can we analyze its military value and make an effective decision. From the perspective of the human vision mechanism, the process of identifying the TOI type is the process of extracting the features of the TOI and comparing them with the known target type information for classification. In this process, the similarity between the image features of the TOI and the known features of the target determines the possibility of the target being identified.

Based on this, the BOVW model was used to estimate the SID of camouflaged vehicles. The algorithm is shown in Fig. 7.

And the algorithm proceeds as follows.

1) Build training datasets: The public images of different camouflage and combat states of vehicles are collected and used as the training set of the BOVW.

2) Local feature selection: Compared with the global features of images selected during CSAD calculation, local features are relatively stable and abundant and used in the BOVM model. Image local feature extraction algorithms include SIFT, SURF, DOG, and MSER. One or multiple algorithms can be selected for fusion. The SIFT feature is selected in the subsequent experiments in this article.

3) Generate a visual dictionary: There are many local feature points in an image, and computing each feature will greatly improve the complexity of calculation, and there are many approximate features. Generally, the clustering algorithm is used
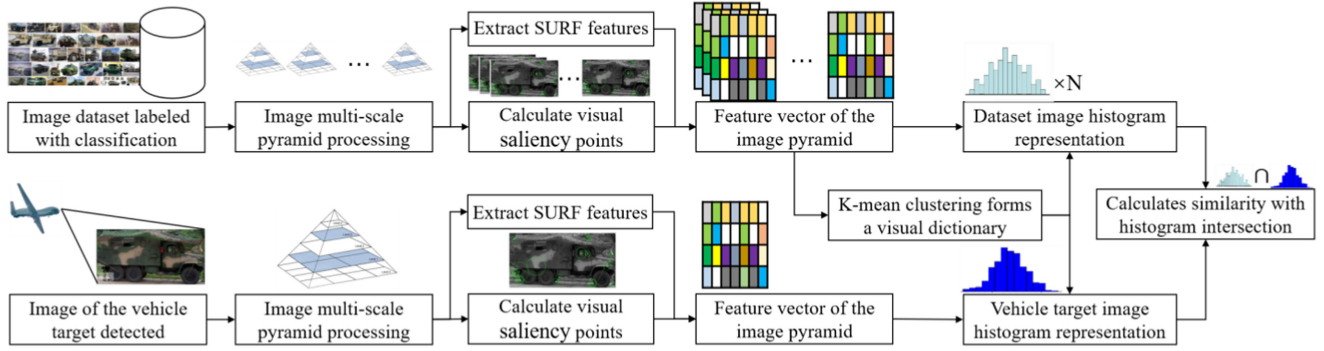
Fig. 7.   Vehicle similarity degree calculation model.

to cluster multiple feature points of the image to reduce the scale of features, which is called the construction of a visual dictionary. The K-means clustering method based on the histogram intersection kernel is used to generate a visual dictionary containing N visual words for extracting SIFT features from images in the training set.

4) Visual dictionary feature construction: To make full use of the spatial information of the image, the multiscale processing of each image is carried out, and the spatial pyramid matching model is adopted to extract the hierarchical information of the high-dimensional local feature space. The visual word nearest to the feature vector of the image in the visual dictionary is calculated. The frequency of visual words appearing in the nearest distance of all feature vectors of the whole image is counted. After normalization, an image feature histogram based on BOVW is obtained.

5) Feature extraction of the camouflaged vehicle image: The pyramid SIFT feature of the camouflaged vehicle image is extracted, the distance between the feature vector and visual word is calculated, the frequency of the nearest visual word is counted, and the histogram of the camouflaged vehicle image feature is obtained after normalization.

6) SID of the camouflaged vehicle: The mean of the intersection between the histogram of the camouflaged vehicle image and the histogram of all the images in the training set is calculated, which is the similarity obtained directly by the algorithm, called algorithm similarity (ASI), represented as Si_A. A certain number of camouflaged vehicle images are collected for the test set to test the algorithm classification. The ratio of correctly classified images to the number of all test images is the accuracy of the algorithm, which is expressed as α. By integrating the accuracy of the algorithm α and the ASI Si_A, the feature similarity of the camouflaged vehicle is defined as

$$Si = (\alpha - \beta) \cdot Si_A + \gamma \cdot (1 - Si_A) \qquad (14)$$

where α is the algorithm accuracy rate, β is the false alarm rate, and γ is the miss rate.

V. Experiment and Results

A. Data Preparation and Processing

1) Background Image and Superpixel Segmentation: Remote sensing background images are selected from the DOTA
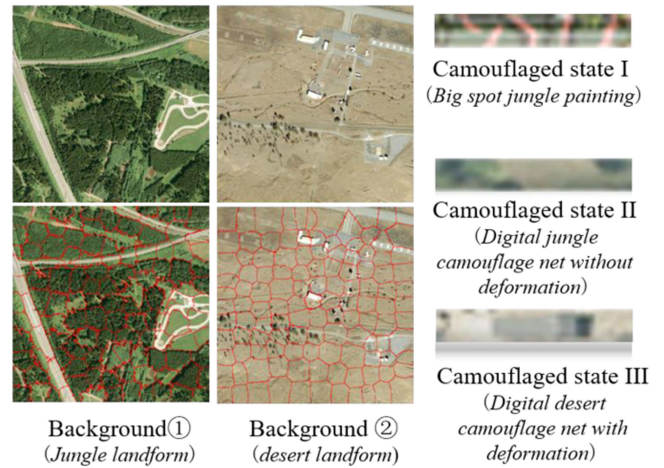

Fig. 8.   Backgrounds and vehicle camouflage states.

remote sensing image target recognition dataset [37], and two ground optical remote sensing images with typical characteristics are taken as examples. Background ① is a summer jungle landform background with a road, and background ② is the Gobi desert background with a cement site.

The original background image to be evaluated with a width of 10 times the vehicle length, a field of view of 200 × 200 m, a size of 2000 × 2000 pi, and a resolution of 254 PPI is captured. According to the number of pixels k = 10 × 10, SLIC segmentation is performed on the background, as shown in Fig. 8(a).

2) Camouflaged Vehicle Image Selection: A certain vehicle is camouflaged in three different states, as shown in Fig. 8(b).

Camouflaged state I: The vehicle has a large spotted jungle camouflage coating.

Camouflaged state II: The vehicle is covered with a full-band digital jungle camouflage net without deformation and expansion.

Camouflaged state III: The vehicle is covered in the full-band digital desert camouflage net and is in the deformation and expansion state.

With the same aerial angle and lighting conditions as the background image, images of three camouflaged states are collected and homogenized into the original target image with a width of 200 pi and resolution of 254 PPI.
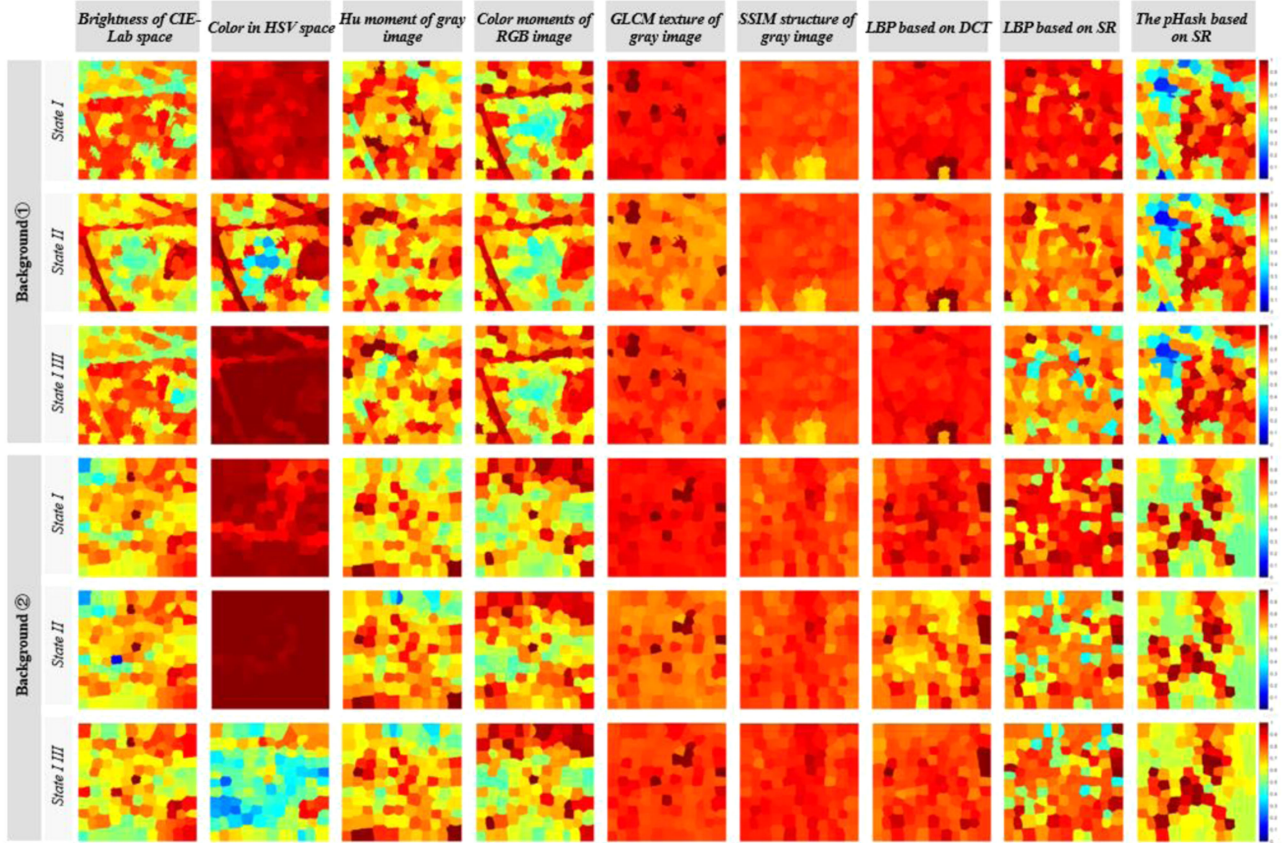
Fig. 9. Saliency thermal maps of 9 features in the 3 camouflaged states under the two backgrounds.

3) Multiscale Image Processing: According to the typical military detection method, three camouflaged state images, and two background images are processed into four different scale images with resolutions of 254, 127, 50, and 25 PPI, respectively, according to the reconnaissance resolutions of 0.1, 0.2, 0.5, and 1 m, respectively, and each layer contains two background images and three camouflage vehicle images.

a) Production of a Vehicle Image Dataset: Three vehicle types, including target vehicles, are selected, and 108 images of different camouflaged states and angles are collected for each type, including 66 images from different media and the internet as the training set and 42 aerial photos as the test set. After clipping, type labels are added and homogenized into a dataset containing 324 images each of 200×200 pi.

B. CSAD Calculation

1) Feature Extraction: According to the nine visual features in 0, feature vectors of three camouflaged vehicle images and feature vectors of all superpixels of two background images are extracted at each scale.

2) TSAD and LSAD Calculation: According to the distance calculation equation of each feature in 0, the feature distance between the camouflaged vehicle and each superpixel is calculated, and TSAD can be obtained according to (3). The feature distance between each background superpixel is calculated, and

the LSAD is obtained according to the adjacent superpixel model and (2).

3) Generate Multifeature Saliency Maps: The LSAD and TSAD of each scale layer are integrated to construct the LSAD and TSAD matrices according to (11) and (12). The CSAD function and (13) are adopted, and the background complex intensity factor σ is set as 1. Each vehicle camouflage image forms a 100×4 CSAD matrix relative to each background image.

The method of coefficient of variation maximization is adopted to screen the CSAD vectors of the four scales in the CSAD matrix, and the vector with the largest coefficient of variation, which is the vector with the largest information content, is selected as CSAD to form a saliency map. Three vehicle camouflage images, 2 background images, and 9 features form a total of 54 saliency maps, as shown in Fig. 9.

In the figure, different colors are used to represent the SAD of the camouflaged vehicle at each superpixel, and blue to red represents the SAD from 0 to 1. It can be seen that the SAD of each feature is different between different backgrounds and vehicles. Under the same background and vehicle, different superpixels represent different landform features, and their SAD also varies greatly.

4) Feature Screening and CSAD Calculation: The nine visual features reflect the vehicle's salience in the background image from different angles, but each feature has a great difference. The complex correlation coefficient method (CRR) and
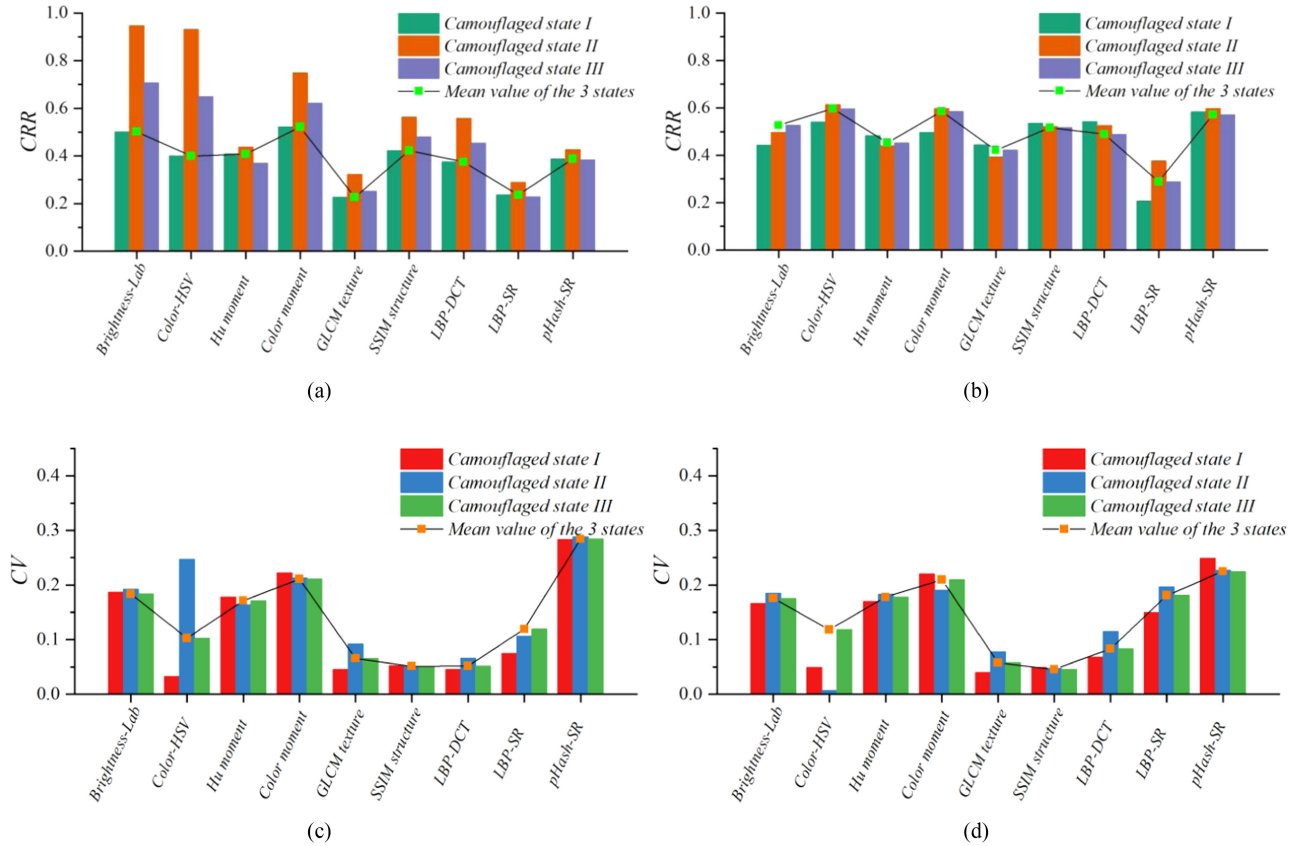
Fig. 10. CRR and CV of the CSAD for 9 features. (a) CRR of each feature in Background ①. (b) CRR of each feature in Background ②. (c) CV of each feature in Background ①. (d) CV of each feature in Background ②.

TABLE III
EFFECTIVE FEATURES AFTER SCREENING AND CSAD

Background	Camouflaged state	Effective features	CSAD
①	I	Brightness-Lab, Hu moment, Color moments, LBP-SR, pHash-SR	0.704
①	II	Color-HSV, Hu moment, Color moments, LBP-SR, pHash-SR	0.663
①	III	Brightness-Lab, Hu moment, Color moments, LBP-SR, pHash-SR	0.771
②	I	Brightness-Lab, Hu moment, Color moments, LBP-SR, pHash-SR	0.690
②	II	Brightness-Lab, Hu moment, Color moments, LBP-SR, pHash-SR	0.727
②	III	Color-HSV, Hu moment, Color moments, LBP-SR, pHash-SR	0.572

the coefficient of variation method (CV) are used to analyze and screen the features, as shown in Fig. 10. The complex correlation coefficient threshold is set at 0.9, and the coefficient of variation is set at 0.85. Redundant features with a complex correlation coefficient greater than 0.9 and features with low information content with a coefficient of variation less than 0.85 are eliminated. The remaining effective features after screening are shown in Table III.

Due to the inhomogeneity of the complex landform background, the SAD of each effective feature on the background superpixel is different, and the SAD entropy information content on the feature dimension is different. Therefore, the entropy weight method is adopted to determine the weight of the effective feature, and the CSAD on each superpixel is calculated by weighting [4]. The mean value of CSAD in the background superpixels is the overall CSAD of the camouflaged state in the background. According to this, the CSAD of three

camouflaged states on two backgrounds can be obtained, as shown in Table III.

C. SID Calculation

1) Feature Extraction and Accuracy Calculation: The SIFT feature vectors were extracted from 324 images of three types of vehicles in the dataset, and the gradient direction and size were calculated according to 16×16 pixel sliding window intervals of 8 pixels. A total of 576×180 128-D feature vectors were extracted from each 200×200 pixel image.

The 103680 feature vectors were iteratively clustered to 300 128-D visual word vectors by the k-means method. The Euclidean distance between each image feature vector and 300 visual word vectors in the dataset was calculated, and the frequency of visual words with the shortest Euclidean distance
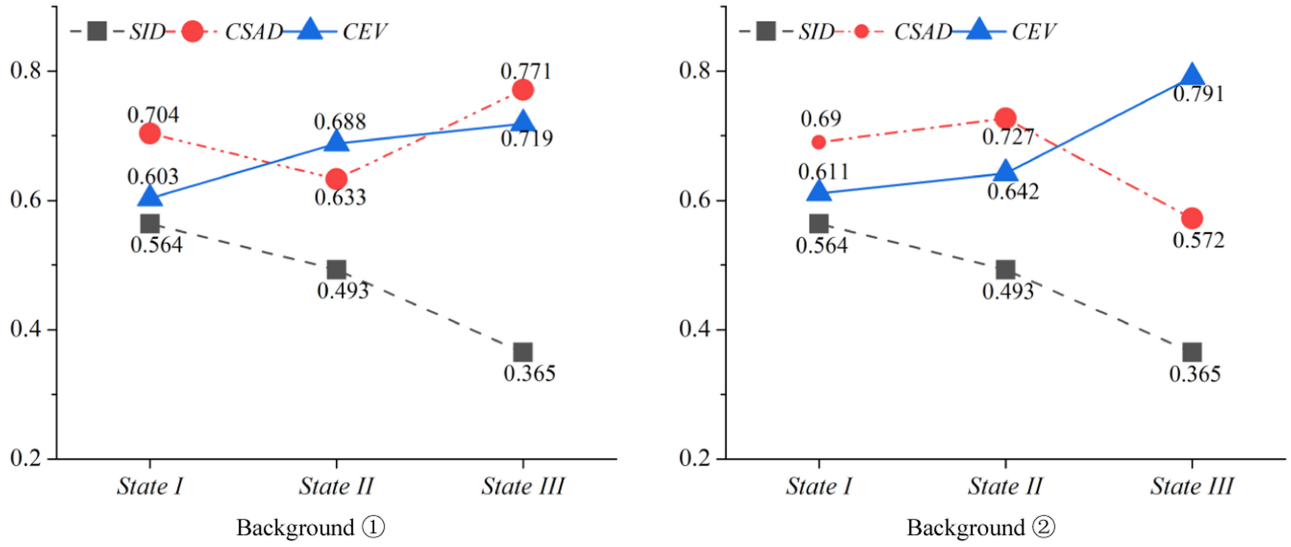
Fig. 11. Comprehensive significance calculated with the entropy weight method.

TABLE IV
ACCURACY RATE OF THE SID ALGORITHM

Vehicle type	Identified as A Number	Identified as B Number	Identified as C Number
A	33	6	3
B	5	30	7
C	4	7	31
Accuracy rate α		0.857	
False alarm rate β		0.107	
Miss rate γ		0.214	

was counted to form the initial feature histogram of the image containing 300 intervals.

The 576 windows of the image were divided into 4×4, 2×2, and 1×1 regions to form a three-layer pyramid structure. The initial feature histograms were calculated by stratification and partitioning to form pyramid feature histograms of 16×300, 8×300, and 1×300 in a total of 21 dimensions and 300 intervals. After normalization, the image feature histograms of the 6300 regions were formed.

The feature histogram of 3×42 images in the testing set was intersected with the histogram of 3×66 images in the training set, and the average value of the intersection was calculated. The type with the largest mean value was taken as the model classification result of the test images. The 126 images in the test set were divided into three types. The ratio of the number of images classified correctly to the number of corresponding types of test images is the type prediction accuracy of the model, as shown in Table IV.

2) SID Calculation: The SIFT features of the three type A camouflaged vehicle states were extracted to obtain their image feature histograms, and the intersection was obtained for each type A image feature histogram of the training sets, which is the Si_A ASI.

The vehicle selected in the experiment is type A, and the accuracy rate α is 0.857, false alarm rate β is 0.107, and miss rate γ is 0.214, were obtained for the algorithm, as shown in Table IV.

ASI calculation results Si_A of the three camouflage states are 0.653, 0.521, and 0.281.

Equation (14) is used for the SID calculation with different camouflaged states of the vehicle, SID calculation results Si of the three camouflage states are 0.564, 0.493, and 0.365.

D. Camouflage Effect Analysis

According to the CSAD and SID calculation results, the CEV of the three camouflaged states under two backgrounds can be obtained according to (1), as shown in Fig. 11.

1) Advantageous Application Environment Analysis: As seen from Fig. 11, for background ①, a CSAD value of 0.633 is achieved using camouflaged state II (i.e., vehicle II); this value is lower than that of the other two vehicle states, indicating that the state of the vehicle that is covered with the full-band digital jungle camouflage net has a better camouflage effect in the forest landform, and the advantageous application environment of camouflaged state II is a landform environment similar to that of background ①. For background ②, the lowest CSAD of 0.572, is achieved using camouflaged state III (i.e., vehicle III), indicating that the relatively advantageous application environment of camouflaged state III is the landform environment similar to that of background ②. At the same time, we see that the advantageous application environment of camouflaged state I in the two backgrounds is not obvious. Based on this, the advantageous application environment of various camouflaged states can be determined, and the camouflaged states with lower SAD can be selected according to the mission landform features to improve the environmental adaptability and camouflage effectiveness of the vehicle.

2) Advantages and Disadvantages Analysis of the Camouflaged States: As seen from the CEV of the three camouflaged states in the two backgrounds in Fig. 11, the CEV of the camouflaged state III vehicle is high under both backgrounds, indicating that after the vehicle is covered with camouflage nets and deformed, it has a good camouflage effect in both backgrounds, and the probability of being detected and identified is lower than that of the other two states.
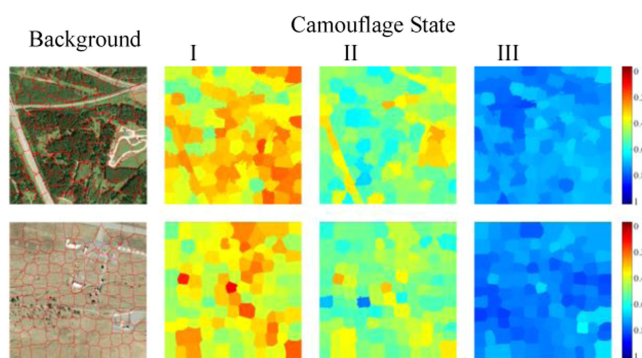
Fig. 12.   CEV of each camouflaged state in the background superpixels.

Taking the CEV of camouflaged state I as a reference value, in background ①, the CEV of camouflaged state II increased from 0.603 to 0.688, an increase of 14.1%. In background ②, when camouflaged state III was covered by the desert camouflaged net and deformed, the CEV increased from 0.611 to 0.791, an increase of 29.5%, which is due to the decrease in SID from 0.564 to 0.365. In background ①, the CEV of camouflaged state III was 0.719, which is significantly better than the value of 0.688 achieved using camouflaged state II, which has a low SID. Even in the disadvantageous application environment of camouflaged state III, masking the similarity features can still better reduce the identified probability and improve the camouflage effect.

The results of the data analysis are consistent with the experience of camouflage practice, indicating that this method can objectively evaluate the camouflage effect of vehicles under different backgrounds, and determine the advantageous application environment of different camouflaged states.

3) Vehicle Concealed Area Analysis: According to the CSAD of each background superpixel and SID of different camouflaged states, the CEV of each camouflaged state in the background superpixels can be obtained according to (1), as shown in Fig. 12.

As seen from this figure, the CEV of different camouflaged states on each background superpixel varies greatly, and different landform backgrounds have a significant impact on CEV.

There is an obvious road in the lower left of background ①, which is divided into seven adjacent superpixels. The mean value of the CEV of the three camouflaged states on these seven superpixels is calculated, and the values of state I, state II, and state III are 0.354, 0.515, and 0.821, respectively. This shows that camouflaged state III has a better camouflage effect when the vehicle is moving or hiding on the road.

In contrast, if the vehicle adopts camouflaged state I or II and moves in background ①, it should avoid the road as much as possible and choose other areas with better CEV to reduce its probability of detection and identification.

Through the analysis of camouflage effects, the CEV of vehicles in different camouflaged states varies significantly under different backgrounds. Vehicles can reduce the CSAD by being covered with camouflage nets, reducing the SID by changing camouflage shapes, and significantly improving camouflage effectiveness. Covering or deforming similar features of vehicles can more effectively improve the camouflage effect and reduce the probability of being identified.

VI. CONCLUSION

In this article, a vehicle camouflage effect evaluation method based on the TLS model in complex landform backgrounds is proposed, the method is verified by calculation, and the results are analyzed. The method extracted features from 2-D images of the background and camouflaged vehicles. Combined with the target reconnaissance process of TLS, the evaluation method of the vehicle camouflage effect was constructed from two aspects: 1) the CSAD of the camouflaged vehicle relative to the background and 2) the SID of the camouflaged vehicle. This method can objectively evaluate the camouflage effect of vehicles under different geomorphic backgrounds and provide data support for the vehicle operation environment, covert area, and camouflaged state selection.

REFERENCES

[1] P. Lanillos, E. Besada-Portas, J. A. Lopez-Orozco, and J. M. De la Cruz, "Minimum time search in uncertain dynamic domains with complex sensorial platforms," *Sensors*, vol. 14, no. 8, pp. 14131–14179, 2014.
[2] D. Hong et al., "Interpretable hyperspectral artificial intelligence: When nonconvex modeling meets hyperspectral remote sensing," *IEEE Geosci. Remote Sens. Mag.*, vol. 9, no. 2, pp. 52–87, Jun. 2021.
[3] D. Hong et al., "More diverse means better: Multimodal deep learning meets remote-sensing imagery classification," *IEEE Trans. Geosci. Remote Sens.*, vol. 59, no. 5, pp. 4340–4354, May 2021.
[4] T. C. Edwards, R. H. Vollmerhausen, R. G. Driggers, and E. Grove, "NVESD time-limited search model," *Infrared Imag. Syst.: Des., Anal., Model., Testing XIV*, vol. 5076, SPIE, 2003, pp. 53–59.
[5] X. Wu, W. Li, D. Hong, R. Tao, and Q. Du, "Deep learning for unmanned aerial vehicle-based object detection and tracking: A survey," *IEEE Geosci. Remote Sens. Mag.*, vol. 10, no. 1, pp. 91–124, Mar. 2022.
[6] O. A. Meykar, "Definitions of effectiveness terms: A report on the purpose and contents of MIL-STD-721B," *IEEE Trans. Aerosp. Electron. Syst.*, vol. AES-3, no. 2, pp. 165–170, Mar. 1967.
[7] J. Xu, Y. Li, and H. Zhang, "Evaluation of optical camouflage effect of air defense missile equipment," *LASER Infra*, vol. 49, no. 5, pp. 95–100, 2019.
[8] Q. Jia, X. L. Lv, W. D. Xu, and J. H. Hu, "Intelligent design of gradual disruptive pattern painting and comparison of camouflage effectiveness," *Cluster Comput.*, vol. 22, no. 4, pp. 9293–9301, 2019.
[9] X. Wu, D. Hong, J. Chanussot, Y. Xu, R. Tao, and Y. Wang, "Fourier-based rotation-invariant feature boosting: An efficient framework for geospatial object detection," *IEEE Geosci. Remote Sens. Lett.*, vol. 17, no. 2, pp. 302–306, Feb. 2020.
[10] Z. Tong, C. Can, F. W. Xing, H. H. Qiao, and C. H. Yu, "Improved small moving target detection method in infrared sequences under a rotational background," *Appl. Opt.*, vol. 57, no. 31, pp. 9279–9286, 2018.
[11] H. Zhu et al., "Multispectral camouflage for infrared, visible, lasers and microwave with radiative cooling," *Nature Commun.*, vol. 12, no. 1, pp. 1–8, 2021.
[12] X. Wu, D. Hong, and J. Chanussot, "Convolutional neural networks for multimodal remote sensing data classification," *IEEE Trans. Geosci. Remote Sens.*, vol. 60, 2022, Art. no. 5517010.
[13] D. Zhao, S. Liu, X. Yang, Y. Ma, and W. Chu, "Research on camouflage recognition in simulated operational environment based on hyperspectral imaging technology," *Spectroscopy*, vol. 2021, pp. 1–9, 2021, doi: 10.1155/2021/6629661.
[14] A. Zavvartorbati, H. Dehghani, and A. J. Rashidi, "Evaluation of camouflage effectiveness using hyperspectral images," *J. Appl. Remote Sens.*, vol. 11, no. 4, 2017, Art. no. 045008.
[15] D. Hong, L. Gao, J. Yao, B. Zhang, A. Plaza, and J. Chanussot, "Graph convolutional networks for hyperspectral image classification," *IEEE Trans. Geosci. Remote Sens.*, vol. 59, no. 7, pp. 5966–5978, Jul. 2021, doi: 10.1109/TGRS.2020.3015157.
[16] Q. Kang, D. Li, K. Guo, J. Gao, and Z. Guo, "Tunable thermal camouflage based on GST plasmonic metamaterial," *Nanomaterials*, vol. 11, no. 2, 2021, Art. no. 260.
[17] Y. Qiao, Z. Meng, P. Wang, and D. Yan, "Research progress of bionic adaptive camouflage materials," *Front. Mater.*, vol. 8, 2021, Art. no. 79.

[18] D. Hong et al., "SpectralFormer: Rethinking hyperspectral image classification with transformers," *IEEE Trans. Geosci. Remote Sens.*, vol. 60, Jul. 2022, Art. no. 5518615, doi: 10.1109/TGRS.2021.3130716.

[19] T. N. Volonakis, O. E. Matthews, E. Liggins, R. J. Baddeley, N. E. Scott-Samuel, and I. C. Cuthill, "Camouflage assessment: Machine and human," *Comput. Ind.*, vol. 99, pp. 173–182, 2018.

[20] R. Achanta, A. Shaji, K. Smith, A. Lucchi, P. Fua, and S. Su¨sstrunk, "SLIC superpixels compared to State-of-the-Art superpixel methods," *IEEE Trans. Pattern Anal. Mach. Intell.*, vol. 34, no. 11, pp. 2274–2282, Nov. 2012.

[21] L. Itti, C. Koch, and E. Niebur, "A model of saliency-based visual attention for rapid scene analysis," *IEEE Trans. Pattern Anal. Mach. Intell.*, vol. 20, no. 11, pp. 1254–1259, Nov. 1998.

[22] D. Qian, Y. Zhou, Y. Wei, and C. Zhang, "Graph laplacian based visual saliency detection," in *Proc. 4th Int. Conf. Digit. Home*, 2012, pp. 201–205, doi: 10.1109/ICDH.2012.30.

[23] X. Hou and L. Zhang, "Saliency detection: A spectral residual approach," in *Proc. IEEE Conf. Comput. Vis. Pattern Recognit.*, 2007, pp. 1–8, doi: 10.1109/CVPR.2007.383267.

[24] R. Achanta, F. Estrada, P. Wils, and S. Süsstrunk, "Salient region detection and segmentation," in *Computer Vision Systems*, (Lecture Notes in Computer Science), vol. 5008, A. Gasteratos, M. Vincze, and J. K. Tsotsos, Eds., Berlin, Heidelberg: Springer, 2008.

[25] R. Achanta, S. Hemami, F. Estrada, and S. Susstrunk, "Frequency-tuned salient region detection," in *Proc. IEEE Conf. Comput. Vis. Pattern Recognit.*, 2009, pp. 1597–1604, doi: 10.1109/CVPR.2009.5206596.

[26] S. Goferman, L. Zelnik-Manor, and A. Tal, "Context-aware saliency detection," *IEEE Trans. Pattern Anal. Mach. Intell.*, vol. 34, no. 10, pp. 1915–1926, Oct. 2012.

[27] R. Achanta and S. Süsstrunk, "Saliency detection using maximum symmetric surround," in *Proc. IEEE Int. Conf. Image Process.*, 2010, pp. 2653–2656, doi: 10.1109/ICIP.2010.5652636.

[28] F. Perazzi, P. Krähenbühl, Y. Pritch, and A. Hornung, "Saliency filters: Contrast based filtering for salient region detection," in *Proc. IEEE Conf. Comput. Vis. Pattern Recognit.*, 2012, pp. 733–740, doi: 10.1109/CVPR.2012.6247743.

[29] D. Hong, N. Yokoya, J. Chanussot, and X. X. Zhu, "An augmented linear mixing model to address spectral variability for hyperspectral unmixing," *IEEE Trans. Image Process.*, vol. 28, no. 4, pp. 1923–1938, Apr. 2019.

[30] S. Lee, J. H. Xin, and S. Westland, "Evaluation of image similarity by histogram intersection," *Color Res. Appl.*, vol. 30, no. 4, pp. 265–274, 2005.

[31] J. Flusser, B. Zitova, and T. Suk, *Moments and Moment Invariants in Pattern Recognition*. New York, NY, USA: Wiley, 2009.

[32] H. Yu, M. Li, H.-J. Zhang, and J. Feng, "Color texture moments for content-based image retrieval," in *Proc. Int. Conf. Image Process.*, vol. 3, 2002, pp. 929–932, doi: 10.1109/ICIP.2002.1039125.

[33] C. G. Eichkitz, J. Amtmann, and M. G. Schreilechner, "Computation of grey level co-occurrence matrix (GLCM) attributes in single and multiple directions," *First Break*, vol. 38, no. 3, pp. 57–62, 2020.

[34] Z. Wang, A. C. Bovik, H. R. Sheikh, and E. P. Simoncelli, "Image quality assessment: From error visibility to structural similarity," *IEEE Trans. Image Process.*, vol. 13, no. 4, pp. 600–612, Apr. 2004.

[35] T. Ahonen, A. Hadid, and M. Pietikainen, "Face description with local binary patterns: Application to face recognition," *IEEE Trans. Pattern Anal. Mach. Intell.*, vol. 28, no. 12, pp. 2037–2041, Dec. 2006.

[36] Z. Li, Y. Zhaohui, Z. Zongtan, and H. Dewen, "Salient region detection using diffusion process on a two-layer sparse graph," *IEEE Trans Image Process*, vol. 26, no. 12, pp. 5882–5894, Dec. 2017.

[37] G.-S. Xia et al., "DOTA: A large-scale dataset for object detection in aerial images," in *Proc. IEEE/CVF Conf. Comput. Vis. Pattern Recognit.*, 2018, pp. 3974–3983, doi: 10.1109/CVPR.2018.00418.

Qinhe Gao received the Ph.D. degree in electromechanical integration from the Xi'an JiaoTong University, Xi'an, China, in 2003.

He is currently a Professor with the Vehicle Evaluation Group, Xi'an Research Institute of High Technology, Xi'an, China. His main research interests include electromechanical system virtual design and simulation, complex system virtual maintenance analysis, and evaluation of vehicle viability.

Zhihao Liu received the Ph.D. degree in mechanic engineering from the Xi'an Research Institute of High Technology, Xi'an, China, in 2018. His main research focuses on simulation of the non-linear dynamics of the high speed ride comfort.

Yao Ding received the M.S. degree in information and computing science in the Key Laboratory of Optical Engineering, Xi'an Research Institute of High Technology, Xi'an, China, in 2013, where he is currently working toward the Ph.D. degree in computer science with the School of Key Laboratory of Optical Engineering

His research interests include neural network, computer vision, image processing, and hyperspectral image clustering.

Tong Huang received the M.S. degree in armament science and technology from the North University of China, Tai Yuan, China, in 2019, where he is currently working toward the Ph.D. degree in armament science and technology with the Xi.an Research Institute of High Technology, Xi'an, China.

His research interests include the antidamage capability evaluation and evaluation of vehicle viability.

Dong Wang received the M.S. degree in aerospace engineering from the Xi'an Research Institute of High Technology, Xi'an, China, in 2011, where he is currently working toward the Ph.D. degree in armament science and technology with the School of Key Laboratory of Armament Science and Technology.

His research interests include vehicle camouflage performances and survival effectiveness evaluation.

Lei Gao received the M.S. degree in vehicle engineering from the Xi'an Research Institute of High Technology, Xi'an, China, in 2020, where she is currently working toward the Ph.D. degree in armament science and technology with the School of Key Laboratory of Armament Science and Technology.

Her research interest include the evaluation of vehicle dynamic performance.